Energy 248 (2022) 123626

Contents lists available at ScienceDirect

Energy

journal homepage: www.elsevier.com/locate/energy

The energy, exergy, and techno-economic analysis of a solar seasonal residual energy utilization system

Datong Gao, Trevor Hocksun Kwan, Maobin Hu, Gang Pei*

Department of Thermal Science and Energy Engineering, University of Science and Technology of China, Hefei, 230027, China

ARTICLE INFO

Article history:
Received 8 October 2021
Received in revised form
6 February 2022
Accepted 28 February 2022
Available online 1 March 2022

Keywords:
Solar energy
District energy system
Energy management strategy
Techno-economic analysis

ABSTRACT

Building heating projects lead to massive energy consumption and carbon emissions. Despite solar energy being clean and abundant for building heating, it has a temporal mismatch issue in which the energy demand and provision are opposite in magnitude between the heating and non-heating seasons. This paper propounds an energy management strategy, which aims to use year-round solar energy efficiently by producing heat in the heating season and generating electricity from the non-heating season's solar residual energy. The results prove that it can meet most of the space heating demand of the target district and provide extra electricity in the non-heating season. The year-round solar effective utilization duration is elevated to 2.48-fold of the conventional solar heating project and the annual thermal energy storage efficiency of 91.22% manifests that solar energy can be utilized more efficiently than the seasonal storage system (< 60%) throughout the whole year. Furthermore, the life cycle cost analysis indicates that the unit energy cost of this system (0.102 €/kWh) is lower than the solar seasonal energy storage system. Therefore, the solar energy supply-demand mismatch problem is settled via this energy management strategy and it is prospective to be promoted worldwide in the future.

1. Introduction

Building energy consumption occupies a large proportion of the total energy consumption. In 2018, up to 293 EJ/year of energy consumption in China occurred in buildings, which accounts for about 21.7% of the total energy consumption [1], and similar trends are taking place in many other countries around the globe [2]. Space heating has occupied a large proportion of the total residential energy consumption [3] and it has a great impact on carbon emission [4]. Based on the statistical data in Fig. 1, most provinces with serious residential building carbon emissions are highly related to building energy consumption. China has put forward the "carbon neutrality" goal to restrain the carbon emission magnitude. However, the energy for space heating is mostly being supplied by fossil fuel power plants in China (about 76% from coal and 4% from oil [5]), which is worsening environmental and climatic issues [6].

The viable solution used for the massive building energy consumption is the efficient and appropriate utilization of renewable energy [8]. Solar energy is a burgeoning energy source for direct building space heating applications [9]. Nonetheless, the solar irradiance resource has a downside of its intermittent behavior, where the demand for space heating and the available solar energy resource always has a seasonal temporal mismatch problem [10]. That is, solar energy is usually adequate in the non-heating season but the space heating demand occurs in the heating season. For example, Fig. 2(a) shows the monthly space heating demand and typical solar irradiation in Helsinki, Finland, whose non-heating season's average irradiance is much higher than in the heating season and the opposite trend occurs on the heat demand. And similarly, for some major Chinese cities exhibited in Fig. 2(b), solar irradiation also has a considerable discrepancy between the non-heating and heating seasons.

The aforementioned problem will lead to a significant amount of solar seasonal residual energy being unemployed, i.e., a mass of solar energy in the non-heating season will be wasted since the supply-demand mismatch problem and converted into waste heat to raise the atmospheric air temperature. More energy is needed for cooling to obtain a comfortable living condition, thereby causing more fossil energy consumption. This is the so-called solar energy "thermal pollution" phenomenon. Besides, the year-round utilization ratio of solar collectors is low since they are also unemployed in the non-heating season. For solving the above problem, the

* Corresponding author.
E-mail address: peigang@ustc.edu.cn (G. Pei).

https://doi.org/10.1016/j.energy.2022.123626
0360-5442/

Nomenclature

Symbols

A	area, m^2
C	cost, €
c_p	specific thermal capacity, J/(kg•K)
Ex	exergy, J
f	solar fraction, %
h	enthalpy, J/kg
I	solar irradiation, W/m^2
J	daily average solar irradiation, $J/(m^2•d)$
L	electricity load, kWh
m	mass flow rate, kg/s
M	mass, kg
n	number
N	lifespan of the system, year
Q	energy, J
r_d	discount rate, %
r_i	inflation rate, %
T	temperature, K
T_i*	normalized temperature difference, $K•m^2/W$
V	price of electricity, €/kWh
w	power of work, W

Abbreviations

DES	district energy system
FBM	factor of bare module
HTF	heat transfer fluid
ORC	organic Rankine cycle
PEC	purchase equipment cost
PWF	present worth factor

Subscripts

amb	ambient
aux	auxiliary energy
ch	charge
col	solar collector
d	design value
disch	discharge
el	electricity
eq	equipment
eva	evaporator
Gen	generator
hd	space heating demand
i	inlet
j	j_{th} time point
k	k_{th} device
l	layer
l_1	the first layer
l_2	the second layer
l_3	the third layer
o	outlet
p	pump
pl	pipe loss
rep	replacement
s	solar
SF	solar field
sh	space heating
sol-pow	solar to power
sys	system
tank	thermal storage tank
th-pow	thermal to power
Tur	turbine
w	water

Greek letters

α_{CF}	factor of the contingency fees
η	efficiency

proper management of solar energy resources in the whole year and making energy supply to users in line with their actual demand are key factors during the solar projects design and implementation.

1.1. Related works

The district energy system (DES) is a viable solution for the solar mismatch issue that has a quasi-autarkic energy system located near the users [12], thus the long-distance thermal energy transport problem is avoided [13]. The DES is more efficient and environment-friendly than the traditional heating strategy (such as central heating and mass power generation) [14]. It can easily make energy adjustments and compensation whenever the energy demands unexpectedly fluctuate. One of the primary motivations of the modernization DES is to be integrated with the renewable energy source [15]. This target is progressively being realized by many researchers by improving the renewable energy share in the heating supplement sector [16]. The various representative studies that are concerned about the solar mismatch problem in DES are summarized in Table 1 and reviewed as below.

The solar seasonal storage method is deemed as a common DES to tackle this temporal mismatch problem [17]. It collects solar energy in the non-heating season while the excess energy is stored in a certain long-term energy storage medium. Then, the stored heat is later discharged to meet the space heating demands of the heating season. Currently, many solar seasonal storage methods have already been proposed, such as the borehole thermal energy system [18], hot water thermal storage [19], water gravel pit storage [20], and so on. Many district energy system (DES) designs based on the solar seasonal storage method have been proposed to satisfy the space heating demand. Paiho et al. [21] presented a seasonal heat storage design for Finland which has achieved around 60% self-sufficiency. Jradi et al. [22] studied the soil-based thermal energy storage system in Denmark. However, the required long-term storage mediums are usually very costly and have a large heat loss during the seasonal transition. Notably, the temperature in the long-term storage device first rises in the non-heating season and then falls throughout the heating season progressively [23]. Therefore, the heat supplement capacity inevitably declines and may be unable to meet the heating demands at later periods of the heating season. Some researchers have developed the high energy storage capacity material for seasonal energy storage [24], but the cost and life cycle stability are still immature for practical applications.

Implementation of various advanced control methods and strategies in DES are powerful measures for solving this solar mismatch problem. For example, virtual storage [25] or combined passive thermal mass and active storage in buildings [26] can optimally reschedule building heating systems. An overview that considers the demand side management techniques for district heating is conducted in Ref. [27]. The different control strategies,

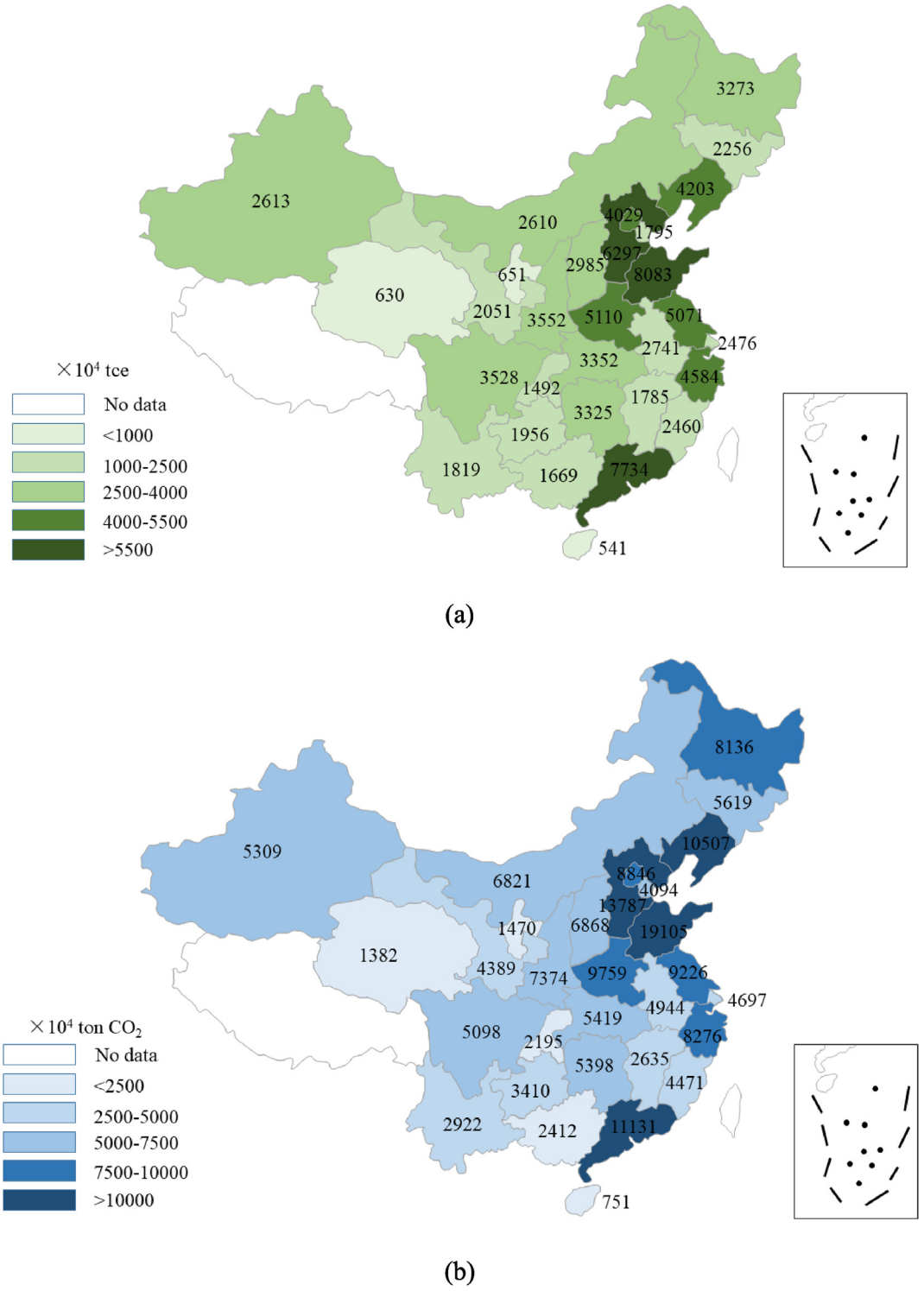

Fig. 1. Annual statistic data (a) residential building energy consumption and (b) residential building carbon emission [5]. *Note: "tce" is the ton standard coal equivalent unit and 1 tce = 2.927 × 10^{11} J.*

such as penalty signal [28], data-driven heating optimization [29], model predictive control [30] will all have remarkable effects for reducing the peak heating load and obtaining desired users' demand profile. However, most of these studies are only focused on the demand side and have seldom considered the renewable energy supplement fluctuation. The combination design of renewable supplements and users' demand should be overall considered [31,32].

The system flexibility in the solar heating-based DES is also getting more and more attention for mitigating the intermittent behavior of solar energy. Generally, the system flexibility is sourced from the building mass [33], energy storage [26], and fluid pipelines

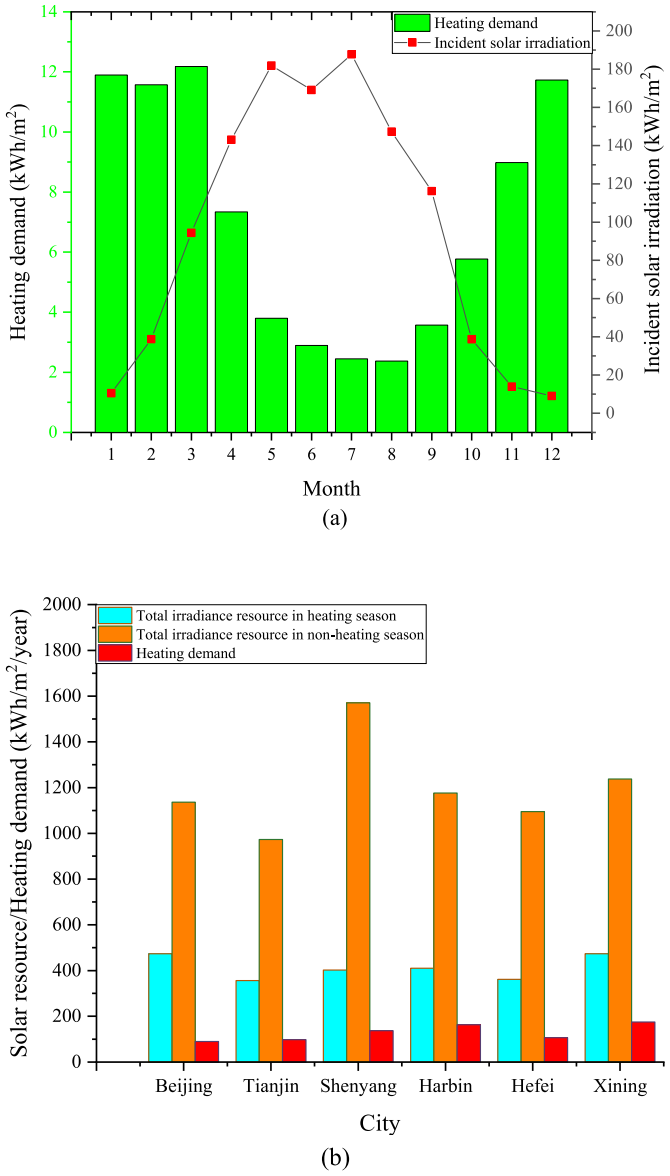

Fig. 2. The energy data. (a) The heating demand and solar irradiation in Helsinki, Finland [10], and (b) space heating demand of some Chinese cities [11].

[34]. Improving the flexibility in energy systems is a promising way to improve the solar energy penetration at the district level [35]. Nevertheless, the energy system flexibility is more effective for solving the short-term rather than the seasonal solar mismatch phenomenon [27].

In addition, some studies are devoted to DES design and energy management. A year-round solar heating system design is proposed to generate heat for space heating in winter and low-pressure process steam for industrial applications in the non-heating seasons. For achieving this purpose, an absorption-compression heat pump is adopted for mode switch in different seasons [36]. Similar to this problem, the researchers in Denmark put forward a solar-driven bifunctional absorption chiller for the heating and cooling demand in a hospital [37]. Furthermore, they also investigated the effect of different solar collectors [38] and system configurations for this seasonal mismatch problem [39].

1.2. Our contributions

Given the existing problems of current solutions discussed above, such as the long-term energy storage losses, unable full use of seasonal residual solar energy utilization, unfitness for the residual buildings, a more appropriate energy management strategy is desired to balance the solar energy between the non-heating and heating seasons urgently. To find a compromise solution for the solar temporal mismatch problem and fill the gap of year-round solar energy utilization methods, an alternative energy management strategy is proposed for solar seasonal residual energy utilization by introducing a proper system design and an energy management strategy to manually reallocate the temporal flow of energy and thus exploit its utilization potential maximally. It aims to supply heat in the heating season preferentially and exploit the solar seasonal residual energy in the non-heating season for producing electricity. The electricity generation in the non-heating season is very meaningful because, as shown in Fig. 3, the electricity load profile during the non-heating season of Beijing, China is typically tremendous [42]. Accordingly, the electricity produced from the aforementioned residual heat can relieve the peak load pressure of the power grid. Via implementing the above energy management strategy, only short-term energy storage is required which has much less heat loss and lower maintenance costs in the DES applications. Moreover, the solar energy resource during the whole year has been utterly utilized whilst the energy demand for the residual building is satisfied to the maximum extent.

To prove the superiority and feasibility of the above year-round solar energy management strategy, an illustration system is proposed with this strategy implementation. The energy and exergy performance, such as thermal efficiency, supplement heating temperature, exergy performance during the whole year, etc. are analyzed to demonstrate its ability to cover the space heating demand and shave the peak load of the power grid in the non-heating season. Then, the annual energy and exergy performance of the illustration system is executed for showing its efficient thermodynamic characteristic. Finally, the techno-economic analysis is performed with a life cycle cost model. Therefore, the feasibility of this energy management strategy in the East China area is proved and it is prospective to be extended worldwide in the future.

2. The energy management strategy and system description

The energy management strategy used for the solar seasonal residual energy utilization is depicted in Fig. 4. In the heating season, the strategy contrives to ensure there is enough heat energy for space heating demand preferentially. While in the non-heating season, as the heat demand is much lower, the solar seasonal residual energy is converted into electricity to make compensation for the power grid. Consequently, heat and power are generated asynchronously in the whole year and avoid the waste of seasonal residual solar energy.

Organic Rankine Cycle (ORC) is a prevalent approach for waste thermal energy recycle which is chosen for electricity generation in the strategy. Apart from the power output having a peak shaving effect in the non-heating seasons, more importantly, the working temperature of ORC is usually 100 °C–150 °C that is suitable for district-scale solar energy conversion [43]. Markides et al. [44] have assessed the solar-driven ORC system for domestic use in the UK and further investigated the working fluid and optimal configuration for a year-round operation [45]. Their studies pointed out that the district-scale ORC system is feasible for implementation in the DES.

To meet the above strategy requirements, the solar collector for year-round solar energy harvesting should be qualified to serve as

Table 1
Representative works for solar heating system modeling and projects.

Research content	Method	Published year	Ref.
Seasonal thermal energy storage equipped with heat exchangers and/or heat pumps in a district heating system	Simulation	2020	[17]
Solar thermal and solar PV combined with ground source heat pump and borehole thermal storage for district heating	Simulation	2017	[21]
Underground soil-based thermal energy storage system for solar energy storage, coupled with a combined heat and power generation system to provide the space heating and domestic hot water demands of the residential project	Simulation	2017	[22]
Borehole thermal energy storage for the heating system of a school building, and combined with the gas boiler or heat pump	Simulation	2018	[23]
Operation results of a 500000 m^3 borehole thermal energy storage for urban district heating	Experiment	2020	[40]
Annual measured thermal performances of a hybrid solar collector field with 5960 m^2 flat plate collectors and 4039 m^2 parabolic trough collectors in Taars, Denmark	Experimental and simulation	2017	[41]
Optimally rescheduling building heating systems for demand side management in district heating networks for desired heating demand profile	Experimental and simulation	2019	[25]
A systematic experiment study for the better heat demand response via taking advantage of demand-side resources to achieve real-time energy supply-demand balance sustainably	Experimental	2020	[26]
Using system optimization and power-flow calculations to analyze the energy interaction between the solar energy and demand side of a district solar-based energy system in Tibet	Simulation	2021	[31]
District energy management optimization strategies that control both the solar supply and the energy demand for the heat generation	Simulation	2019	[32]
Assess the potential of buildings to modulate the heating demand and proposed control strategies to exploit the flexibility potential considering both energy and thermal comfort	Simulation	2016	[33]
Presents a possible definition of flexibility and its sources in a thermal network. Gives the important means to cope with the intermittent generation of renewable energy heat sources	Review	2018	[35]
System modeling for generating high-temperature heat for space heating in winter and low-pressure process steam for industrial applications in other seasons	Simulation	2021	[36]
System modeling of a bifunctional solar assisted absorption chiller that produces cooling in summer and contributes massive heat for district heating purposes during the other months	Simulation	2017	[37]

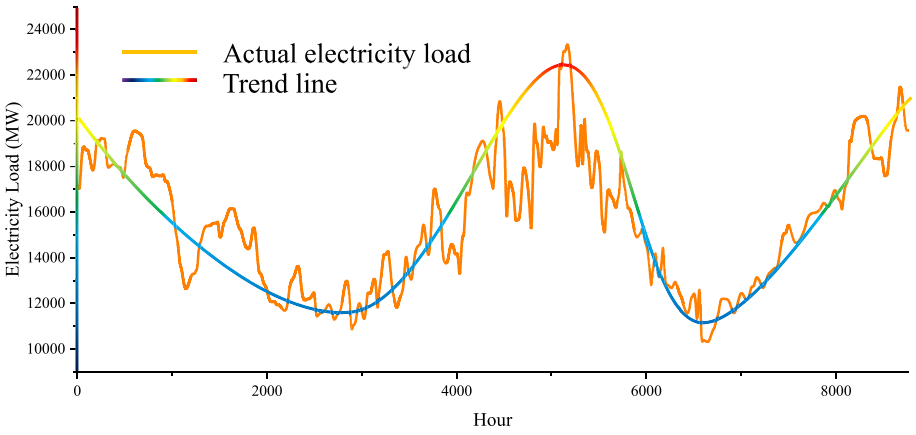

Fig. 3. The annual electricity load profile of Beijing, China [42].

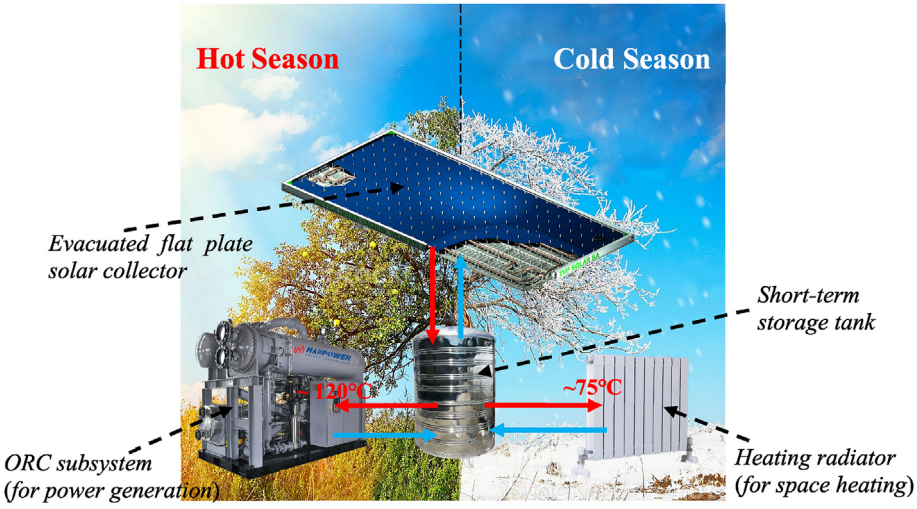

Fig. 4. The schematic of the solar seasonal residual energy utilization system.

both the low and medium-temperature heat sources. Generally, the parabolic trough collector can meet this demand but it can only harvest the beam solar irradiation and the tracking device is also required [46]. Since solar diffuse irradiation in the regions that need space heating usually accounts for a large proportion of total solar irradiation, the non-concentrating solar collector is much more proper for this strategy. Hence, a novel highly efficient evacuated flat plate solar collector is adopted [47]. This solar collector is eligible since it can efficiently serve as a low-temperature heat source (50–100 °C) to space heating in the heating season and yield medium-temperature (100–180 °C) thermal energy for thermal electricity conversion in the non-heating season. Thus, the problems of tracking device requirement together with diffuse irradiation unexploited of parabolic trough collector are also solved.

To validate the superiority of the solar seasonal residual energy utilization strategy, this paper uses an illustration system shown in Fig. 5, which consists of three subsystems. I: evacuated flat plate solar collectors array, II: ORC subsystem, and III: heat supplement subsystem (encompass a short-term thermal storage tank to avert the bad weather). Taking the Beijing, China region as an example, the illustration system's operation strategy within a year is set as follows.

(1) Mode 1, Space heating: Subsystem I and III are running during the heating season (from 15th, Nov. To 28th, Feb. of next year);
(2) Mode 2, Power generation: Subsystem I, II, and III are running during the non-heating season (from 1st, Mar. To 14th Nov.).

In compliance with the statistical information of Fig. 6, the typical hourly electricity load of Beijing, China varies with time periodically by day. It can be noticed that the peak electricity load of the non-heating season turns up from 17:00 to 22:00 in both the weekend and workday, so the running time of the ORC subsystem is restricted in that time slot for peak shaving. To prevent the frequent start and shut down of the devices, the evaporating temperature of the ORC unit is set to work between the 100–120 °C, thus the working condition of the ORC unit components are basically at their

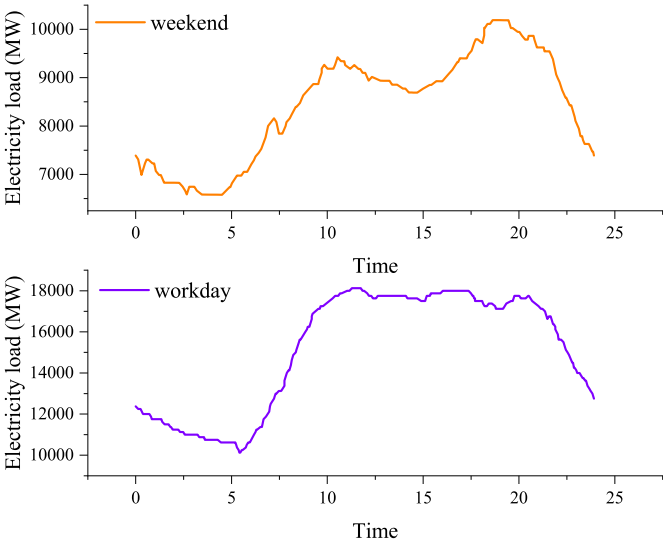

Fig. 6. The typical electricity load profile of Beijing, China at the weekend and the workday [42].

design point. The reason for choosing this temperature range comes from the comprehensive consideration of the solar collector and ORC unit's thermodynamic traits. The main design and operation parameters are exhibited in Table 2.

To substantiate the superior thermal performance of the evacuated flat plate solar collector in the whole year and demonstrate its qualification for this energy management strategy, a systemic experiment (Fig. 7) is executed in this study where an elaborate description of the corresponding platform can be found in Ref. [47].

3. Methodology

In this section, the calculation methodology for the entire system's component in Section 2 is established. The performance indicators of the solar field are clarified and the space heating demands of users are predicted by a validated model. Then, each

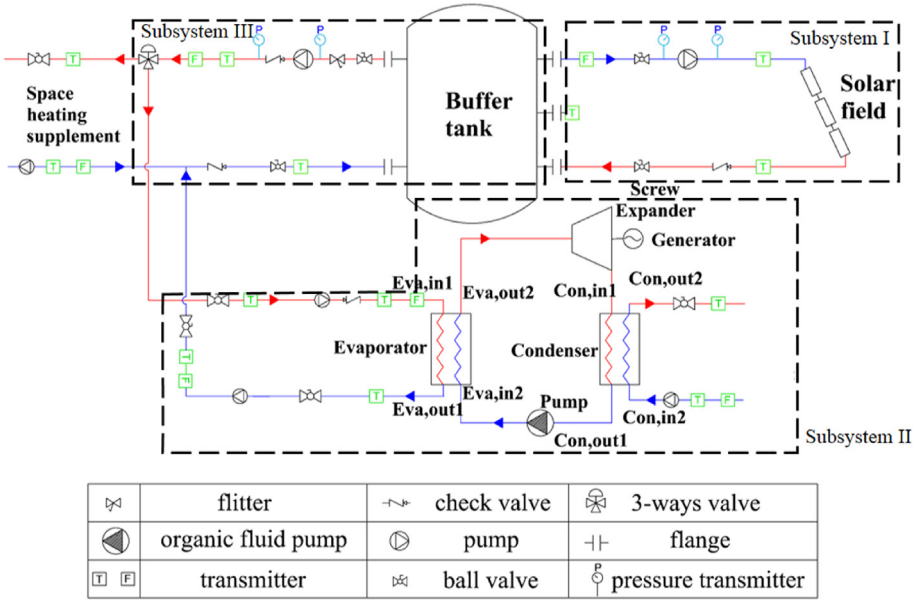

Fig. 5. The schematic of the illustration system.

Table 2
The basic working parameters of each subsystem.

Items	Value
Target space heating area/(m^2)	14000
Space heating inlet temperature/(°C) [48]	75
Space heating outlet temperature/(°C) [48]	50
Expander's isentropic efficiency [49]	0.85
Generator's efficiency [50]	0.95
Pump's efficiency [51]	0.85
heat exchanger pinch point/(K) [52]	5
Design solar irradiation/(W/m^2)	800
Working fluid of ORC unit	R245fa
The design inlet temperature of ORC subsystem/(°C) [53]	120
The design outlet temperature of ORC subsystem/(°C) [53]	100

component's configuration (such as the ORC generation unit and storage tank, etc.) is designed and optimized for users subsequently. Next, an exergy efficiency indicator is defined for useful energy analysis in the whole year. Finally, a tech-economic analysis model is also developed to confirm the feasibility of this system.

3.1. The evacuated flat plate solar collector platform

The experiment of the evacuated flat plate solar collector is carried out in the natural environment so the boundary conditions (such as the solar irradiation, ambient temperature, etc.) are varying at every moment. The normalized temperature difference T_i* is used to describe the thermal performance which involved the inlet temperature, ambient temperature, and solar irradiation at the same time, so it can reflect the thermal efficiency of the solar collector comprehensively [54].

$$T_i^* = \frac{\overline{T_i} - \overline{T_{amb}}}{\bar{I}} \tag{1}$$

The thermal efficiency of the whole solar field is calculated as [55]:

$$\eta = \frac{\overline{m} c_{p,w} (\overline{T_o} - \overline{T_i})}{A_{SF} \bar{I}} \tag{2}$$

For a more accurate result of the evacuated flat plate solar collector, the normalized temperature difference T_i* and thermal efficiency η is tested under steady-state conditions, i.e., select the experiment results that the boundary condition parameters fluctuate in a narrow range at the time of testing.

3.2. The space heating subsystem

A set of 10 typical office buildings were selected for the following study of the illustration system in Beijing, China. Every building has 7 floors with a 200 m^2 heating area on each floor. The windows area occupied about 15% of the south and north facade of the building. A representative architect structure and materials [56] are chosen for the modeling and the space heating demand in the whole year in TNRSYS software. The boundary conditions such as solar irradiation, ambient temperature are taken from the EnergyPlus weather data [57]. The average simulation result of the heating demand is 91.59 kWh/(m^2·yr), which is very close to the real data of 89.85 kWh/(m^2·yr) statistic by the Ministry of Housing and Urban-Rural Development of the People's Republic of China [11]. The relative result is shown in Fig. 8, the heating demand is concentrated between Nov. and Mar. and the total available solar

Fig. 7. The medium-scale experiment platform of the evacuated flat plate solar collector.

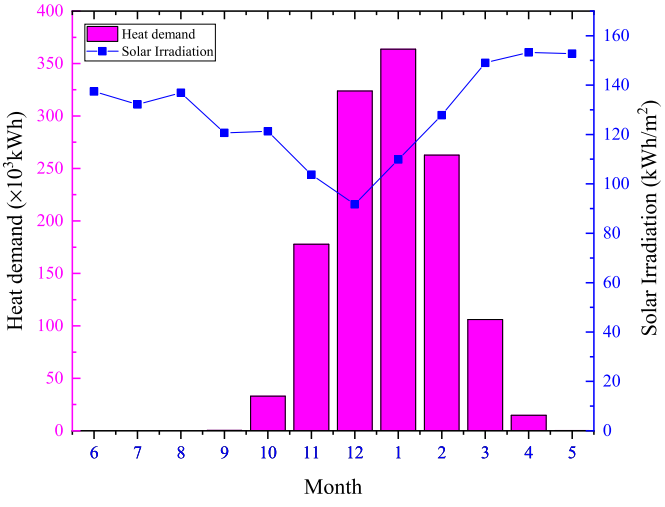

Fig. 8. The heat demand and solar irradiation of Beijing, China.

irradiation is not very weak in the heating season.

The main design principle of the space heating subsystem is according to the heating demand and the National Standard of China. The solar field is designed as [48]:

$$A_{SF} = \frac{86400 Q_{hd} f_d}{J \eta_{col}\left(1 - \eta_{pl}\right)} \tag{3}$$

where η_{pl} is the heat loss of the fluid pipes, value for 0.95 from Ref. [48], and J is the daily average solar insolation in the heating season, value for 10.927×10^6 J/(m^2•d) [58]. f_d is the designed value of the solar fraction, value for 0.6 from Ref. [48]. Since the availability of solar energy is intermittent and unpredictable, it is generally not cost-effective to provide 100% of the energy requirements of a thermal system with solar energy in the whole heating season round [59].

$$m_{col} = \begin{cases} \dfrac{Q_{hd,i}}{c_{p,w}\left(T_{sh,in} - T_{sh,out}\right)} & \left(T_{tank,lay1} \le T_{sh,in}\right) \\ \dfrac{Q_{hd,i}}{c_{p,w}\left(T_{sh,in} - T_{sh,out}\right)} \cdot \dfrac{T_{sh,in} - T_{amb}}{T_{tank,lay1} - T_{amb}} & \left(T_{tank,lay1} > T_{sh,in}\right) \end{cases} \tag{4}$$

where $T_{tank,lay1}$ is the temperature of the fluid which stays in the top layer of the storage tank.

The temperature distribution in the cylindrical stratified water storage tank along the vertical direction is set as 3 layers for simplified analysis. The temperature of each layer can be considered the same and each layer is assumed to exchange energy and mass with the adjacent layers (see Fig. 9). The governing equation of each layer is [60]:

$$\begin{aligned} \frac{M_{tank}}{n_l} c_{p,w} \frac{\partial T_{l1}}{\partial t} &= m_{col} c_{p,w}\left(T_{col,out} - T_{l1}\right) + m_{user} c_{p,w}\left(T_{l2} - T_{l1}\right) - U_L A_{l1}\left(T_{l1} - T_{amb}\right) \\ \frac{M_{tank}}{n_l} c_{p,w} \frac{\partial T_{l2}}{\partial t} &= m_{col} c_{p,w}\left(T_{l1} - T_{l2}\right) + m_{user} c_{p,w}\left(T_{l3} - T_{l2}\right) - U_L A_{l2}\left(T_{l2} - T_{amb}\right) \\ \frac{M_{tank}}{n_l} c_{p,w} \frac{\partial T_{l3}}{\partial t} &= m_{col} c_{p,w}\left(T_{l2} - T_{l3}\right) + m_{user} c_{p,w}\left(T_{user,out} - T_{l3}\right) - U_L A_{l3}\left(T_{l3} - T_{amb}\right) \end{aligned} \tag{5}$$

The heat transfer fluid (HTF) circulation flow rate is controlled according to the outlet temperature of the storage tank and the real-time heat load. When the outlet temperature is higher than the design point, the cold water with the ambient temperature is injected into the pipe to stabilize the temperature and flow rate at the users' end. The flow rate in different conditions can be calculated by the law of energy conservation.

where n_l is the total layers of the stratified water storage tank, U_L is the thermal loss coefficient of the storage tank, value for 2500 J/(hr•m^2•K).

3.3. ORC subsystem

As the strategy mentioned above, the ORC subsystem needs a dynamic control strategy for a better operation, which can be

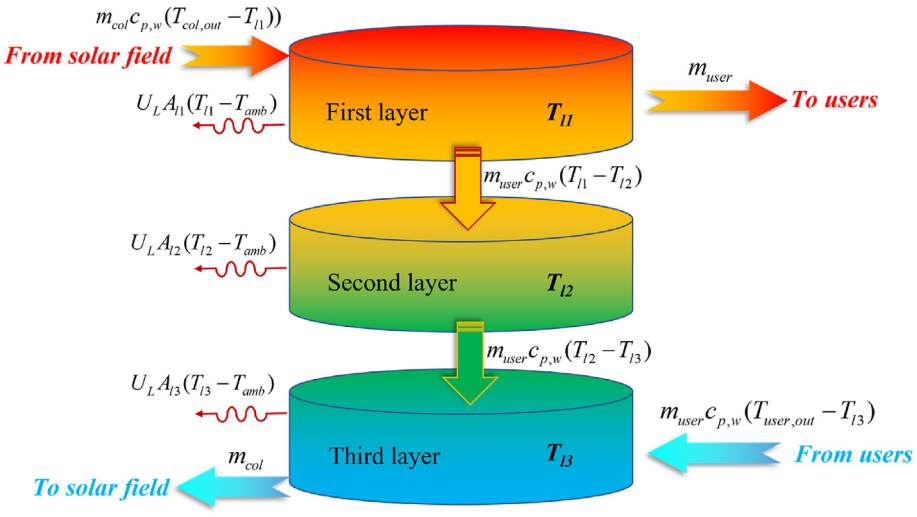

Fig. 9. Discretized control volume analysis of the storage tank.

expressed as follows.

For a certain time j in the non-heating season, if the ORC subsystem is running in the time j-1, then:

$$\text{at time } j \begin{cases} \text{keep running,} & (T_{l1} > T_{ORC,out,d}) \\ \text{shutdown,} & (T_{l1} < T_{ORC,out,d}) \end{cases} \tag{6}$$

For a certain time j in the non-heating season, if the ORC subsystem is not running in the time j-1, then:

$$\text{at time } j \begin{cases} \text{startup,} & (T_{l1} > T_{ORC,in,d}) \\ \text{keep inoperation,} & (T_{l1} < T_{ORC,in,d}) \end{cases} \tag{7}$$

The solar field needs a certain volume of HTF to sustain a steady operation, so a heat exchanger is desired to transfer heat from the solar field. The energy balance equation of the heat exchanger is [50]:

$$m_{SF}(h_{SF,out} - h_{SF,in}) = m_{ORC}(h_{eva,out2} - h_{eva,in2}) \tag{8}$$

The mass flow of the organic fluid is adjusted according to the temperature in the first layer of the storage tank. All the components of the ORC subsystem are operating close to their designed working condition and avoiding the great fluctuation of the off-design work situation [61].

$$m_{ORC} = \frac{Q_{ORC,d}}{c_{p,w}(T_{l1} - T_{ORC,out,d})} \tag{9}$$

The organic vapor expands to drive the turbine and generator, the work produced by the screw turbine is [50]:

$$w_{Tur} = m_{ORC}(h_{Tur,in} - h_{Tur,out}) = m_{ORC}(h_{Tur,in} - h_{Tur,out,s})\eta_{Tur} \tag{10}$$

where the η_{Tur} is the adiabatic efficiency of the screw turbine.

The detailed ORC calculation model can be found in Ref. [50]. The power produced by the generator is:

$$w_{Gen} = w_{Tur}\eta_{Gen} \tag{11}$$

The power consumed of the pump in ORC is [62]:

$$w_p = m_{ORC}(h_{p,out} - h_{p,in}) = m_{ORC}(h_{p,out,s} - h_{p,in})/\eta_p \tag{12}$$

where the η_P is the adiabatic efficiency of the pump.

The thermal-power and solar-power conversion efficiencies are calculated by Ref. [63]:

$$\eta_{ORC,th-pow} = \frac{w_{Gen} - w_p}{m_{ORC}(h_{eva,out2} - h_{eva,in2})} \tag{13}$$

and

$$\eta_{ORC,sol-pow} = \frac{w_{Gen} - w_p}{IA_{SF}} \tag{14}$$

3.4. Exergy analysis

Since multiple forms of energy are supplied, the exergy is a more convincing indicator to show the ascendancy of this illustration system. In the heating season, the exergy flow is separated into three parts, i.e. the exergy from the solar field, exergy accumulated in the storage tank, and the exergy discharge from the storage tank. In the non-heating season, the third part is the resulting electricity energy.

The exergy from the solar field is [64]:

$$Ex_s = IA_{SF}\left(1 - \frac{4}{3}\frac{T_{amb}}{T_s} + \frac{1}{3}\left(\frac{T_{amb}}{T_s}\right)^4\right) \tag{15}$$

The exergy charged for the storage tank is [65]:

$$Ex_{ch} = m_{col}c_{p,w}\left[(T_i - T_o) - T_{amb}\ln\left(\frac{T_i}{T_o}\right)\right] \tag{16}$$

In line with the above equations, the exergy discharge from the storage tank to users or ORC unit is:

$$Ex_{disch} = \begin{cases} m_{user}c_{p,w}\left[(T_o - T_i) - T_{amb}\ln\left(\frac{T_o}{T_i}\right)\right] & (\text{in the heating season}) \\ w_{Gen} - w_p & (\text{in the non} - \text{heating season}) \end{cases} \tag{17}$$

Correspondingly, the exergy efficiencies of each exergy flow process are defined as [66]:

$$\eta_{ex,SF-ch} = \frac{Ex_{ch}}{Ex_{sol}} \tag{18}$$

$$\eta_{ex,disch} = \frac{Ex_{disch}}{Ex_{ch}} \tag{19}$$

The overall exergy efficiency is:

$$\eta_{ex,sys} = \eta_{ex,SF-ch} \cdot \eta_{ex,disch} \tag{20}$$

3.5. Life cycle cost analysis

The techno-economic performance of the DES is a dominating determinant in the decision-making phase [12]. Some systems which show noticeable environmental benefits end up with uneconomical construction [67]. The life cycle cost analysis method has been employed in many DES analysis studies [68]. It takes into account the time value of cash flow and involves the complete range of costs detailly [59]. The net present value is composed of three parts: the initial cost of equipment, the cost of the whole system operation (equipment maintenance, the electricity consumed of the pump and auxiliary heating energy), and the cost of the equipment replacement (some equipment can't survive for more than the design system's lifespan).

The main equipment in the illustration system is consists of the solar collectors' array, the short-term storage tank, the ORC unit, the pump, and the heat exchanger. Thereinto, the cost the main equipment costs are calculated by Eq. (21) [69].

Table 3
Cost function of the main components.

Components	PEC_k	CAP_k type	Ref.
Solar thermal panels	$974.15 \times CAP_{ST}^{0.833}$	Aperture area (m^2)	[69]
Pump	$389 \times \ln\left(\frac{CAP_{pump}}{1000}\right) - 283.15$	Flow rate (kg/h)	[70]
Heat exchanger	$CAP_k \cdot 10^{3.13 \times (\log 10^{CAP_{HE}})^{-0.331}}$	Heat exchange area (m^2)	[71]
Storage tank	$3955.3 \times CAP_{tank}^{0.653}$	Volume (m^3)	[69]
Auxiliary boiler	$225.01 \times CAP_{tank}^{0.746}$	Power (kW)	[71]
ORC Turbine	$2237 \times CAP_{tur}^{0.41}$	Power (kW)	[72]
ORC pump	$1026 \times \left(\frac{CAP_{pump}}{300}\right)^{0.25}$	Power (kW)	[73]
ORC Condenser	$338.6 \times CAP_{con}$	Heat exchange area (m^2)	[73]
ORC Evaporator	$216.6 + 353 \times CAP_{eva}$	Heat exchange area (m^2)	[74]

$$C_{eq} = (1 + \alpha_{CF}) \cdot \sum_k (PEC_k \cdot FBM_k),$$
$$k \in \{\text{solar collectors, short} - \text{term storage tank, pump and the heat exchanger}, \cdots\} \quad (21)$$

where α_{CF} is the factor of the contingency fees, the *PEC* is the net purchase equipment cost and the *FBM* refers to the cost from transportation to installation. The detailed equation of each parameter can be found in Table 3.

The operating cost in the lifespan is calculated in accordance with the total electricity consumed by the pump and the auxiliary energy the system cannot provide [75]. These parameters are monitored while the system running.

$$C_p = PWF_p \cdot \sum V_{el,i} L_{p,i} \quad (22)$$

$$C_{aux} = PWF_{aux} \cdot \sum V_{el,i} L_{aux,i} \quad (23)$$

where $V_{el,i}$ is the price of electricity, value for 0.3 €/kWh on average for the study region. $L_{p,i}$ and $L_{aux,i}$ are the real-time pump and heater load for the system, respectively.

The maintenance cost of the equipment is assumed to be proportional to the initial investment cost and increases at a certain rate per year. Since all the operating costs will occur in the future, the present worth factor (PWF) is used for this time effect [59].

$$PWF = \frac{1}{r_d - r_i}\left[1 - \left(\frac{1 + r_i}{1 + r_d}\right)^N\right] \quad (24)$$

where the N is the lifespan of the whole system and it is considered as 20 years, r_d is the discount rate which equals 3.5%, and r_i is the inflation rate which equals 2.3% [69].

Generally, the vulnerable part of the system needs to be replaced regularly, such as the pump, a few pieces of solar collectors, etc. In this system, these components will be replaced two times during the whole lifespan [69].

$$C_{rep} = PVF_n \sum_k (PEC_k \cdot FBM_k), k \in \{\text{solar collectors, pump}, \cdots\} \quad (25)$$

where the PVF_n denotes the cash flow in the n_{th} year amounts to the present value and it can be calculated as follows [59].

$$PVF_n = \frac{(1 + r_i)^n}{(1 + r_d)^n} \quad (26)$$

The net present value is the sum of the above three parts.

3.6. The main assumption and calculation process

For the balance of calculation resources and actual physical process, some assumptions are made in the analysis:

1) All components are operating in the steady-state during each time step [51].
2) The efficiency of the pump, generator, and turbine are constant [50] since the evaporation temperature of the ORC unit is restricted in a narrow slot of its design condition.
3) The heat transfer processes are steady and have constant heat exchange efficiency for each heat exchanger (includes the evaporator, condenser of the ORC unit).
4) The pressure drop, potential energy, and kinetic energy for the HTF of the solar field and ORC unit are omitted [76].

The calculation process is shown in Fig. 10 according to the above numerical model and operating strategy. After loading the database of the meteorological parameters, the storage tank temperature, the solar energy harvesting amount, etc. are calculated hourly in the heating season (blue box). When the solar irradiance is lower than the threshold, the solar field will stop circulating. The heat supplement to users is controlled according to the real-time heating demand. At the end of the heating season, the system is switched to the power generation mode with a higher operating temperature in the solar field (green box). The ORC subsystem is controlled according to the heat accumulated in the storage tank and the electricity load hourly. These models are established in the Matlab environment, and the HTF properties reference the REFPROP database.

4. Results and discussion

4.1. The thermal efficiency of the solar field

The validation experiment of the evacuated flat plate solar collector is conducted in the heating season between 2019 and 2020 with a low ambient temperature. After a long-term experiment, the steady-state test data and the boundary conditions (such as the solar irradiation and ambient temperature) are summarized in Table 4. The normalized temperature difference fitting curve is obtained for characterizing the thermal performance of evacuated flat plate solar collectors.

The fitting curve of the thermal efficiency with respect to the normalized temperature difference is illustrated in Fig. 11. The regression curve equation is obtained as shown in Eq. (27). The intercept efficiency is 90.23% and the heat loss coefficient is 2.6887. It is demonstrated that the evacuated flat plate solar collector has shown high thermal efficiency in the target temperature range needed for this energy management strategy.

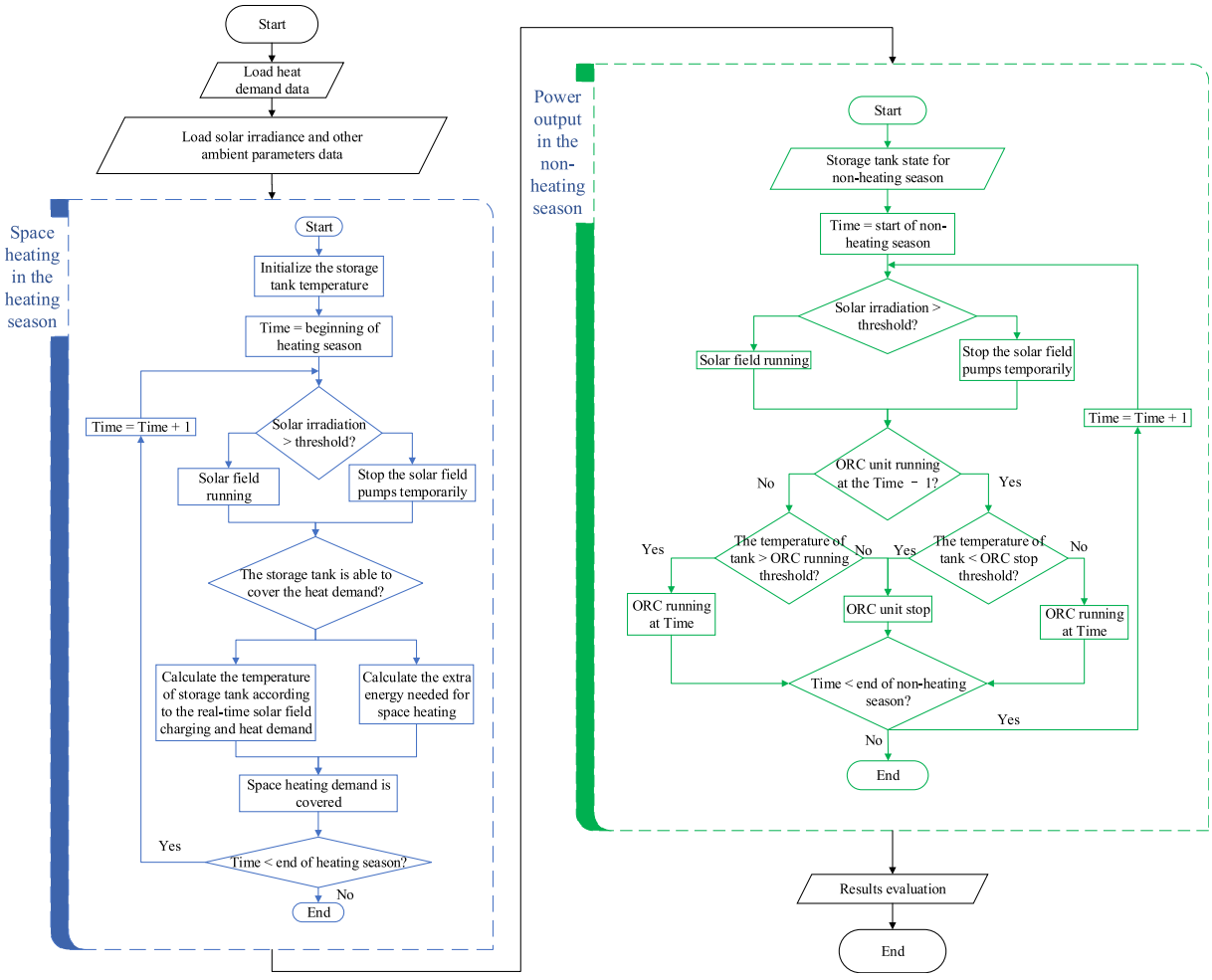

Fig. 10. The flow chart of the calculation process.

$$\eta = 0.9023 - 2.6887T_i^*, \left(R^2 = 0.9269\right) \quad (27)$$

After the space heating circulation, the back HTF usually has a temperature of 50 °C [48]. Under this circumstance, the thermal efficiency of the evacuated flat plate solar collector has reached 76.79% under the condition of solar irradiation is 800 W/m^2 and ambient temperature is 10 °C, which is much higher than other ordinary non-concentration solar collectors [77]. For the ORC power generation, a medium temperature is required to evaporate the working fluid. But the thermal efficiency is still above 50% when the inlet temperature is around 120 °C. What is noteworthy is that these results are acquired under a low ambient temperature that will cause a higher heat loss to the environment. The main reason for the high thermal efficiency is that the high vacuum inside renders a superior thermal insulation effect. Therefore, the studied evacuated flat plate solar collector is very qualified for space heating and ORC power generation purpose in the previously mentioned energy management strategy.

4.2. The thermal performance in the heating season

In light of the space heating subsystem design and the operating strategy, the thermal performance in the whole heating season is presented in Fig. 12 (a). The initial temperature in the storage tank is appointed to the ambient temperature of 15th, Nov. At the beginning of the heating season, the outlet temperature of the storage tank is not sufficient for space heating but it raised very quickly within 72 h. Meanwhile, the thermal efficiency in this stage is also remarkable because of the low inlet temperature. After the temperature attains the setpoint, the heat is provided to users regularly. A little glide is observed in the middle of Jan. That is owing to a few days of bad weather. The heat supply is steady on most occasions in the whole heating season. Finally, in late Feb., as there is a much lower space heating demand, the temperature in the storage tank increases sharply. It can not only meet the requirement of the space heating comprehensively but the temperature goes up with noticeable rapidity to a higher level. In a short-term view, it is prejudicial for the space heating application since the solar collector's thermal efficiency decrease greatly. Nonetheless, with a long-term view, a higher temperature grade is suitable for the ORC unit operation. In line with the operating strategy, the mass flow rate to users will be regulated based on the storage tank's temperature; so the heat supplement temperature at the users' end is still around the target temperature to protect the heating equipment.

Furthermore, it is worth noting that the above results are under the condition that the initial temperature of the storage tank is the same as ambient temperature, i.e., it is the worst situation for this system. In practical applications, the temperature of the storage tank will not fall as low as the surroundings. Thus, it is predictable that this system will have a better performance in continuous

Table 4
Steady-state data of evacuated flat plate solar collector test platform in the heating season.

η	T_{in}	T_{out}	G	T_{amb}	T_i*	m
	°C	°C	W/m^2	°C	K·m^2/W	m^3/h
65.48%	74.09	87.78	702.02	9.24	0.0924	1.34
65.82%	74.16	88.77	745.01	9.74	0.0865	1.34
65.24%	74.23	89.64	792.37	10.45	0.0805	1.34
66.14%	74.36	89.77	781.79	9.98	0.0823	1.34
66.56%	74.37	90.29	802.37	10.58	0.0795	1.34
67.89%	74.57	90.81	802.17	11.61	0.0785	1.34
71.85%	74.77	81.54	746.84	16.13	0.0785	1.32
69.51%	74.81	80.69	669.26	14.72	0.0898	1.34
69.07%	74.83	80.71	673.83	13.94	0.0904	1.34
71.31%	74.87	81.74	764.06	14.88	0.0785	1.32
69.38%	74.98	80.72	655.66	15.79	0.0903	1.34
67.20%	75.07	80.65	652.33	13.89	0.0938	1.34
63.48%	91.53	102.48	768.72	9.02	0.1073	1.33
66.14%	91.86	103.18	664.00	18.11	0.1111	1.33
49.68%	104.97	113.36	550.69	12.83	0.1673	1.32
55.67%	105.12	118.31	771.76	11.31	0.1216	1.32
52.21%	105.24	115.00	609.40	12.98	0.1514	1.32
54.82%	105.28	116.50	667.13	12.49	0.1391	1.32
56.25%	105.38	118.70	771.18	11.96	0.1211	1.32
54.86%	105.39	117.66	728.90	12.36	0.1276	1.32
55.29%	105.39	117.20	696.10	12.83	0.1330	1.32
55.88%	105.60	118.43	747.89	11.94	0.1252	1.32
58.98%	108.35	120.87	890.97	14.32	0.1055	1.32
48.25%	116.68	126.40	649.10	15.19	0.1564	1.31
53.37%	116.87	130.55	825.67	13.36	0.1254	1.31
46.98%	116.90	125.75	606.69	16.21	0.1660	1.31
50.49%	117.09	128.18	707.77	15.49	0.1435	1.31
50.64%	117.15	128.43	717.67	15.59	0.1415	1.31
49.80%	117.15	128.36	726.99	17.58	0.1370	1.32
50.26%	117.30	128.05	691.92	18.17	0.1433	1.32
48.97%	117.33	127.44	667.86	17.64	0.1493	1.32
47.60%	117.41	126.54	620.51	18.33	0.1597	1.32
44.87%	117.46	125.19	558.45	18.77	0.1767	1.32
51.28%	117.47	129.11	733.37	17.75	0.1360	1.32
53.97%	117.50	130.29	762.80	16.26	0.1327	1.31
54.55%	117.50	130.59	772.13	16.49	0.1308	1.31
55.16%	117.54	131.48	813.19	14.43	0.1268	1.31
54.42%	117.61	130.53	764.44	16.22	0.1326	1.31
55.00%	117.64	130.91	776.20	16.51	0.1303	1.31
55.03%	117.77	131.19	785.03	15.96	0.1297	1.31
50.05%	126.17	138.73	800.25	13.82	0.1404	1.30
46.66%	126.60	136.79	696.85	16.90	0.1574	1.30
51.21%	126.63	138.84	759.99	17.34	0.1438	1.30
45.86%	126.73	136.56	683.86	17.00	0.1605	1.30
50.36%	126.80	138.43	736.43	16.98	0.1491	1.30
45.44%	126.86	136.39	668.79	16.98	0.1643	1.30
49.53%	126.87	137.56	688.44	16.52	0.1603	1.30
51.47%	126.88	139.76	797.66	15.57	0.1395	1.30
49.66%	127.01	138.05	709.06	16.56	0.1558	1.30
58.48%	129.98	145.67	942.09	19.82	0.1169	1.31

operation. From another perspective, the thermal efficiencies of the evacuated flat plate solar collector are calculated and distributed in the scatter diagram hourly. It is observed that most efficiencies points are over 60% even in the cold weather.

It is undisputed that the illustration system can meet the most user demands in the heating season without much auxiliary energy consumption. More specifically, the heating capability of this illustration system is shown in Fig. 12(b). Even the initial temperature of the storage tank is set at the ambient temperature and the solar irradiation is relatively weak, the heat demand is satisfied to a great extent with solar energy from Nov. To Jan. Since the solar irradiation increases in Feb., the heat demand can be covered totally by solar energy. The solar fraction in the whole heating season has reached 90.83% and only a few fossil fuels are consumed. In terms of the average solar collectors' thermal efficiency, it surpasses 50% in the first three months but falls in Feb. on account of

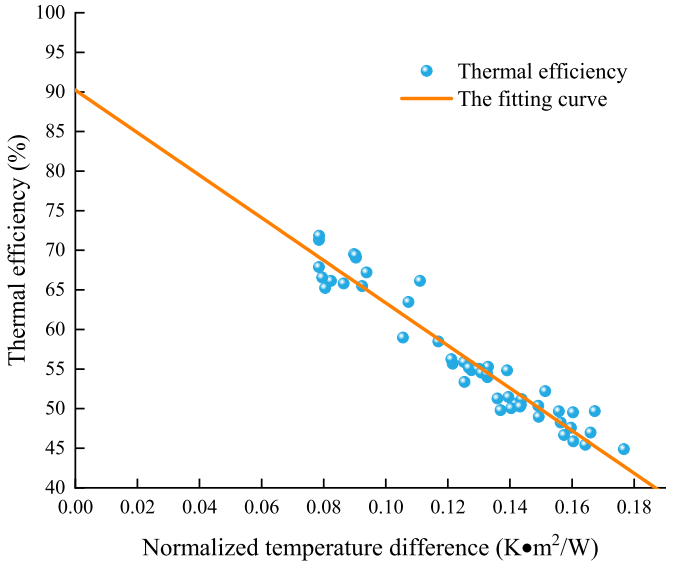

Fig. 11. The thermal efficiency of the evacuated flat plate solar collector under the low ambient temperature condition.

the relatively higher inlet temperature. Fig. 12(c) presents the energy share of each part (during the whole heating season). Most of the energy loss is caused by the solar collector's heat loss. It is comprised of the solar energy loss caused by the thermal radiation when the operating temperature increase and the low solar irradiance magnitude that can be harvested by solar collectors. For more effective vacuum-type solar collection, a further thermal radiation loss recycle process is needed to improve the thermal efficiency. The solar energy losses caused by the storage tank only account for a small share due to the short-term energy storage, and 46.73% of the solar irradiation is efficiently utilized for space heating.

4.3. The power output performance in the non-heating season

In the non-heating season, the solar field is used for the ORC subsystem and its main objective is to make the utmost of the solar seasonal residual energy. To minimize the initial cost of the whole system, the storage tank is identical to the one used in the heating season. In doing so, the temperature in the tank is the same as the ending of the heating season.

Fig. 13 gives the outlet temperature of the storage tank (blue line) and the thermal efficiency of the solar field of each hour (red scatter). It is indicated that during most days of the non-heating season, the ORC subsystem can act as an auxiliary power supply system and the power supply time can be prolonged via the storage tank for a few hours after sunset. The ORC subsystem will briefly halt during certain periods of bad weather, so these days the solar field is only used to elevate the temperature of the storage tank. The red scatters represent the thermal efficiency of the solar field. It is observed that most points range from 40% to 70% notwithstanding the operating temperature of the solar field is over 90 °C, and the average value of the whole non-heating season is 48.49%. These results demonstrate that the evacuated flat plate collector is excelling in the thermal performance compared with other non-concentrating solar collectors in the medium temperature scope. The temperature fluctuates between the setting temperature interval of the ORC subsystem (100–120 °C set in Table 2). Owing to the desired working time slot restriction, the temperature will reach a higher level a few times when solar irradiance is sufficient.

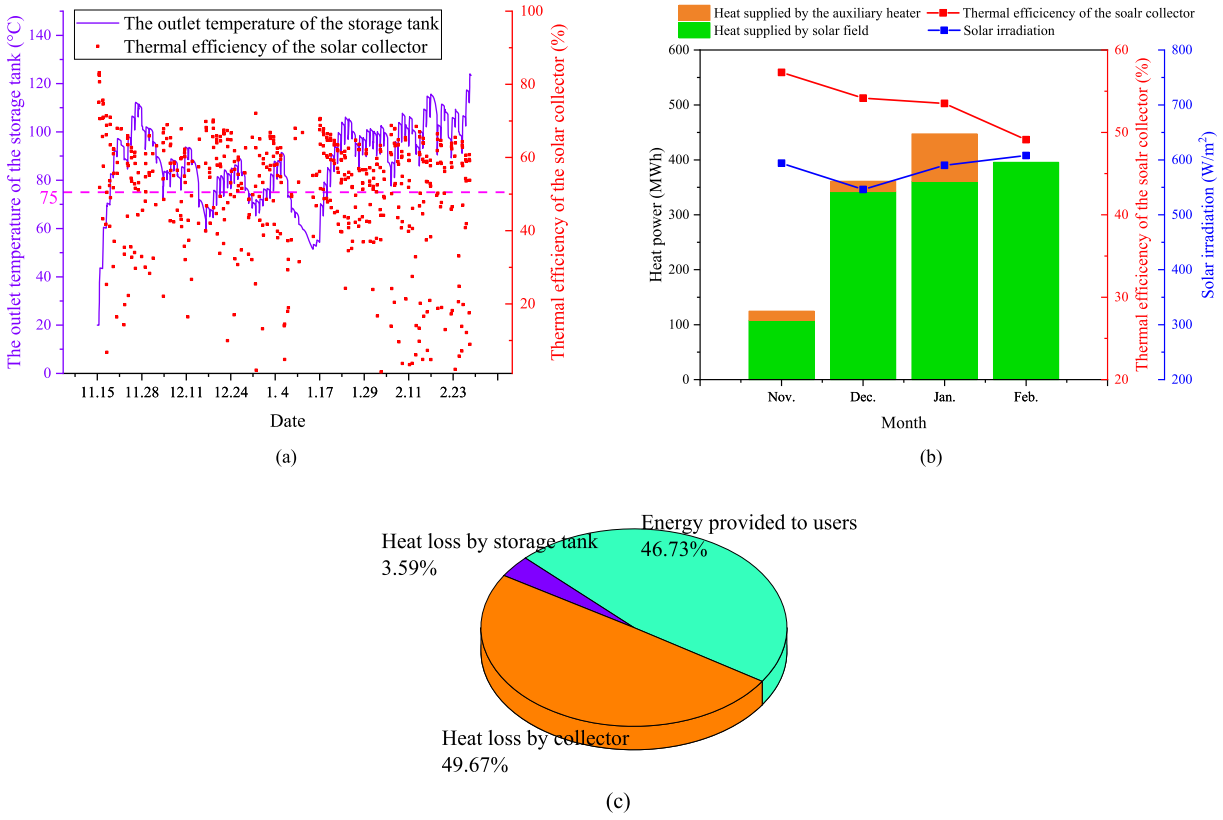

Fig. 12. The thermal performance of the heating season, (a) the output temperature for the space heating and thermal efficiency of evacuated flat plate collector, (b) the capability of the space heating and thermal efficiency in each month, and (c) energy breakdown of the total solar irradiation.

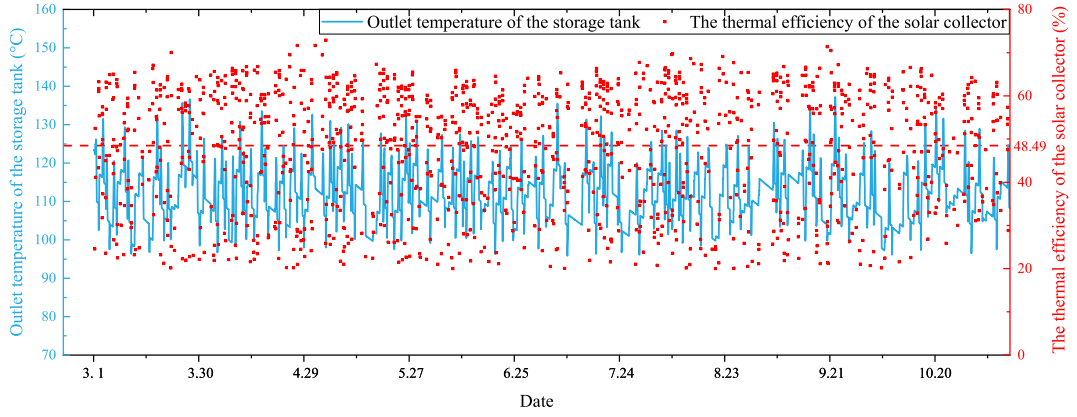

Fig. 13. The outlet temperature of the storage tank for the ORC subsystem and the solar collector's thermal efficiency.

Fig. 14 depicts the monthly electricity output of the ORC subsystem. The electricity output is in correspondence with the thermal energy supplied by the solar field. The total electricity output is 434.53 MWh for the whole buildings and varies marginally in the whole period. However, from the view of thermal efficiency, the average thermal efficiency of the ORC subsystem is around 10% for power generation. The holistic solar-to-power conversion efficiency of the whole system is about 5%. This also can be seen in Fig. 15 which shows the energy share of each part. Unlike the heating season, only 4.61% is used for power generation ascribed to the parasitic characteristics of the ORC. 35.75% of solar energy is lost for the condensation process. This part is useless for the residential buildings in the non-heating season for its low temperature and low heating demand. However, the condensed heat can be used for industrial processes with an auxiliary heat pump if the system is adopted in the industrial sectors, such as drying [78], solar sterilization [79], solar steam generation [36], etc. It is noticed that the solar irradiation loss in the solar field is roughly equivalent to the cold season even if the operating temperature rises. The reason can be attributed to the simultaneous increase of solar irradiation and ambient temperature in the non-heating season. Also, the heat loss proportion of the storage tank is relatively low with common insulation materials.

As shown in Fig. 16, the system's daily energy supply is depicted. It is noticed that solar energy is converted with thermal and electricity output in the whole year. In the heating season, heat is

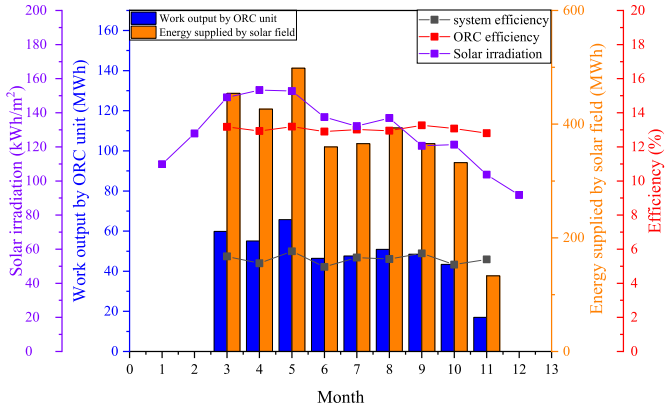

Fig. 14. The power output performance of the ORC subsystem.

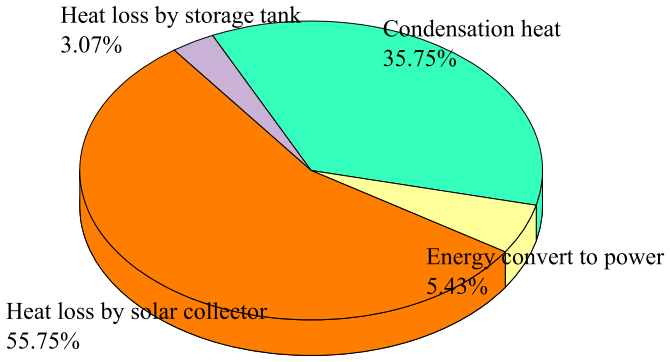

Fig. 15. Energy breakdown of the total solar irradiation in the non-heating season.

discharged from the storage tank uninterruptedly. Hence, the output energy has a relatively higher fluctuation due to the solar irradiation magnitude. While in the non-heating season, due to the running time and evaporation temperature restriction of the ORC subsystem, the daily electricity output fluctuates in a narrow range between 3500 and 5000 kWh. So it can support a steady power supplement for the users at the set time slot. Moreover, this strategy with the ORC subsystem can offset the peak load of electricity, thereby mitigating the burdens of the enormous electricity consumption during the non-heating season.

4.4. Exergy analysis

The daily exergy flow from solar irradiation to the users is exhibited in Fig. 17. On account of the great temperature difference between the sun and heat transfer fluid, about only 10% of solar irradiation exergy are transformed into thermal exergy of heat transfer fluid. Unlike the energy provision, the exergy in the non-heating season is higher than in the heating season. This is because electrical energy is considered as available energy entirely.

From the year-round perspective, the average solar collector exergy efficiency in the whole year (i.e. $\eta_{ex,SF\text{-}ch}$) is 11.04% and the exergy used for space heating and electricity generation efficiency (i.e. $\eta_{ex,disch}$) is 71.78%. Hence, the average system exergy efficiency in the whole year (i.e. $\eta_{ex,sys}$) is 7.93%. Some researchers have also made the investigation of exergy performance of the solar seasonal storage methods, such as H. Ozturk et al. [80] uses a soil packed-bed solar seasonal heat storage. The average exergy efficiency during the charging process (i.e. $\eta_{ex,SF\text{-}ch}$) is 2.03% according to their results. It is noticed that the above efficiency only takes the charging process into account and leaves out the discharge process that causes exergy destruction. The results in Ref. [66] given the exergy efficiency during the charging and discharging process of a central solar heating plant with seasonal heat storage. In their study, the overall exergy efficiency (i.e. $\eta_{ex,dischar}$) is 19% in the yearlong working. Notice that the solar collection process is not considered in their analysis, so the whole systematic exergy efficiency will be comparable with the result in the last study of [80].

4.5. Heat loss analysis

The heat loss caused by the storage tank is presented in Fig. 18.

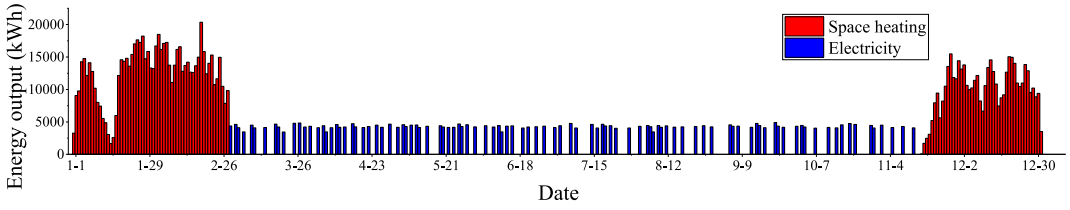

Fig. 16. Daily thermal/electricity provision in the whole year.

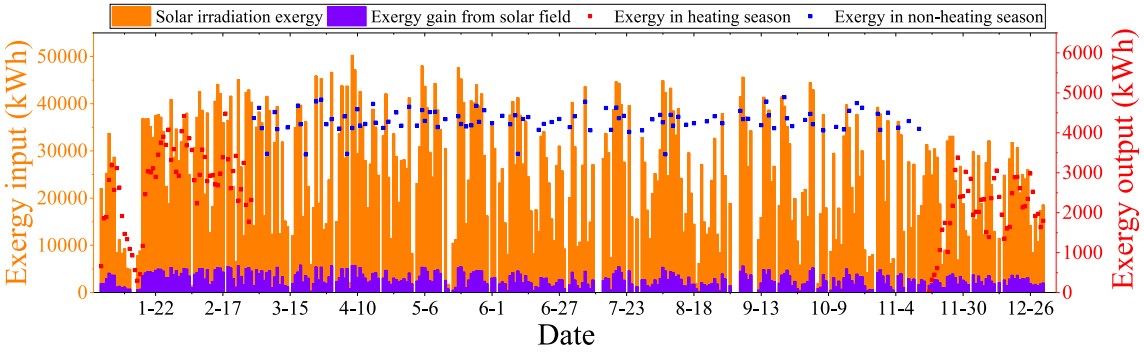

Fig. 17. Exergy flow in the whole year.

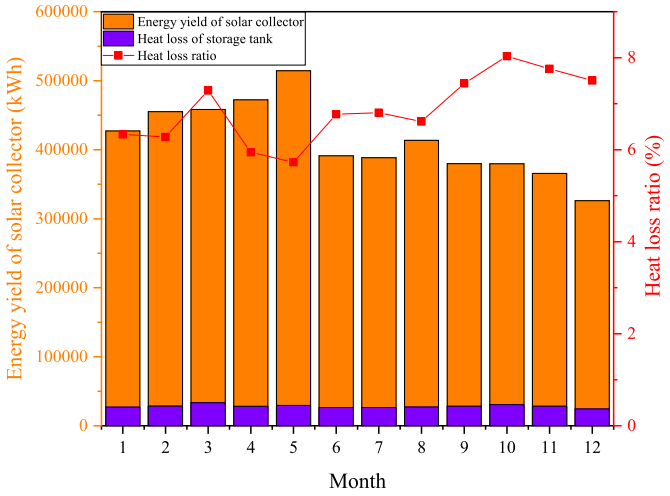

Fig. 18. Heat loss of the storage tank in the whole year.

This energy management strategy uses a short-term energy storage method so the heat loss ratio is as low as 7% around the year. The heat losses are more serious in the heating season even the average temperature in the heating season is lower than in the non-heating season. Another key factor for the heat loss in the storage tank is the real-time energy consumption fitness degree with the solar energy yield, i.e., the shorter energy storage period leads to less energy loss. From the perspective of the whole year, 91.22% of energy yield from solar collectors is transported to the subsequent applications. Hence, solar energy is efficiently delivered and the heat loss in the thermal storage process is inessential in the whole system.

In the solar seasonal storage system, thermal storage over a long period method is significant in the system design process. The long-term storage will cause much higher heat loss amid the transition of seasons. Some studies have investigated the storage efficiency of seasonal storage. For example, the well-known Drake Landing Solar Community in Okotoks, Alberta, Canada had only 40% annual efficiency during 5-years operation [81]. Hirvonen [82] carried out the multi-object optimizations on a borehole thermal energy storage-integrated solar community at a high latitude area. The annual storage efficiency of their result was generally between 40% and 60%. Panno [23] studied a solar seasonal borehole thermal energy system in the Mediterranean area with 59% annual storage efficiency. The use of latent heat and chemical methods for seasonal thermal storage is a promising solution for preventing heat loss but has not progressed on the district level [83].

The storage volume is also a decisive factor in seasonal storage design since it has a great influence on thermal storage efficiency [40]. The large-scale storage volume is under development to increase its efficiency. However, it will vastly limit the system's flexibility in practical applications. Compared with the solar seasonal storage method, the energy management strategy that involves short-term energy storage will be more efficient and flexible.

4.6. The continuous operation

In practical applications, this system will run continually, i.e. all year round. Therefore, the temperature in the storage tank is the same at the transition time of system function alternating. The outcomes of the storage tank's outlet temperature in continuous 3 years are simulated and shown in Fig. 19. At the beginning of each heating season (i.e. the ending of the non-heating season), the outlet temperature of the storage tank is higher than requisite except for the first year, so the insufficient initial heating capacity is made up. Meanwhile, the residual energy in the non-heating season will not be wasted. In terms of the solar energy effective utilization duration (i.e. the total hours of which the solar energy is converted into other energy forms to satisfy the actual energy demand), this energy management strategy will be 2.48-fold compared with the conventional solar space heating projects.

4.7. Techno-economic performance

With the life cycle cost analysis method, the gross cost of the illustration system is analyzed in detail. The cost of each part is exhibited in Fig. 20. It is noted that the solar field and thermal storage tank are the primary cost of the whole system and they account for 34.25% and 17.25% of the total cost, respectively. This is consistent with the most distributed energy system results [59].

According to the life cycle cost analysis, the unit energy cost of the system is 0.102 €/kWh. For a comparative illustration, the two annual energy systems [84] for district heating networks are used as a benchmark example. There, a similar techno-economic evaluation method was used, and their result indicates the unit energy cost of their system is about 0.675 €/kWh which is much higher than the distributed energy system proposed in this paper. Furthermore, other similar studies, such as a solar-assisted seasonal borehole thermal energy system designed for the school heating system in Ref. [23] and a central solar seasonal storage for thermal energy supply in Barcelona, Spain by Tulus et al. [69], report values of 0.121 €/kWh and 0.116 €/kWh with the same system lifetime. To sum up, the illustration system in this paper has a comparable techno-economic performance with the solar seasonal storage method. Moreover, it can supply extra electricity in the non-heating season, so the solar seasonal residual energy utilization strategy is proved to be superior to the solar seasonal storage method.

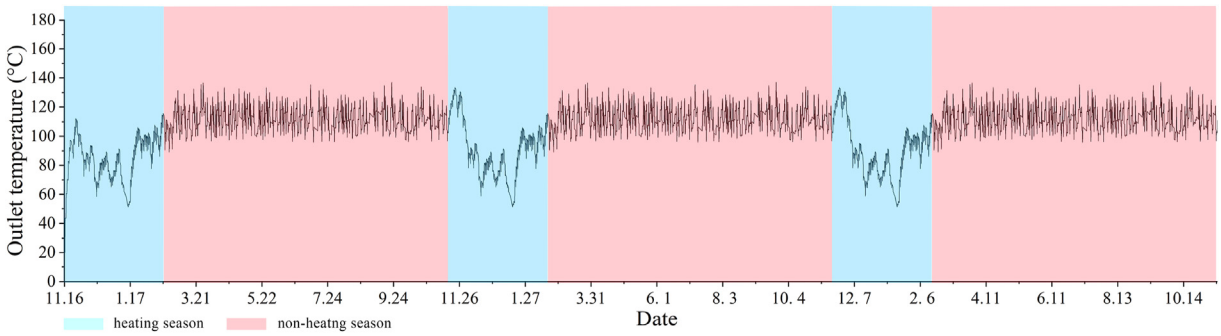

Fig. 19. Outlet temperature from the solar field in continuous 3 years.

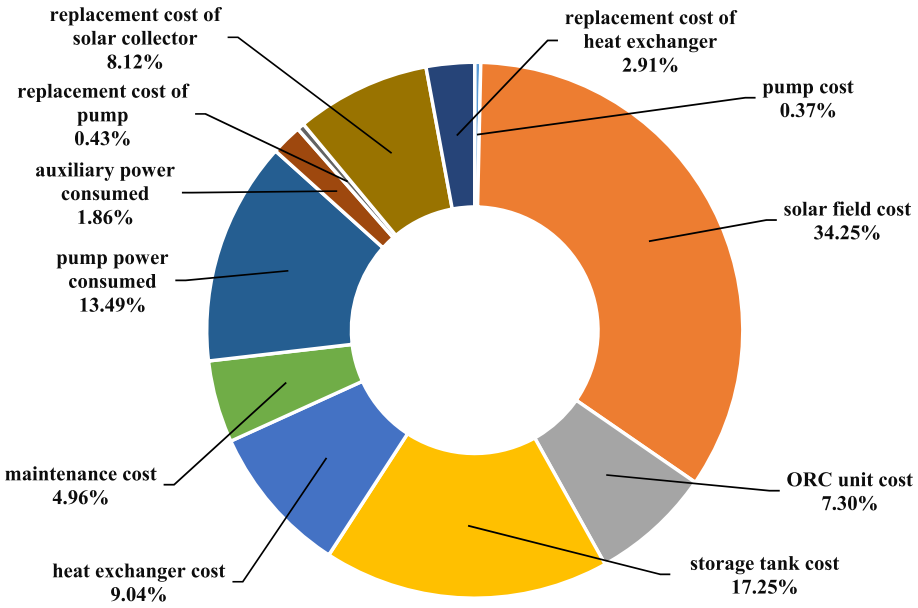

Fig. 20. The breakdown of the life cycle cost of the system.

5. Conclusions

In summary, this paper has realized an all-year-round and efficient solar energy resource utilization by applying a new energy management strategy that supplies heat in the heating season and utilizes the abundant residual energy in the non-heating season for electricity production. The corresponding solar seasonal residual energy utilization system is capable of properly solving the solar seasonal supply-demand mismatch problem of the thriving solar space heating project globally. The main conclusions are summarized as follows.

1. Based on the typical meteorological data of Beijing, China, the illustration system can meet the major space heating demand (solar fraction in the whole heating season has reached 90.83%) of a community-level district and compensate for the peak load of the power grid (total electricity output in non-heating season is 434.53 MWh). The year-round solar effective utilization duration will be 2.48-fold of the conventional solar space heating projects.
2. The short-term thermal storage brings a high energy storage efficiency (91.22%) to the illustration system. For this reason, the size of this district energy system can be saleable depending on the target energy supply area and avert the vast heat loss (generally over 40%) in seasonal thermal storage systems. Therefore, it will be more efficient and flexible in practical applications.
3. The annual exergy efficiency is up to 71.78% of the thermal charging and discharging process, which allows more solar energy converted to useful energy in the whole year and avoids the “thermal pollution” caused by the otherwise waste solar seasonal residual energy.
4. In comparison with the solar seasonal storage method, the unit energy cost of the illustration system is 0.102 €/kWh which is lower than the solar seasonal storage system. Moreover, extra electricity is obtained in the non-heating season that further enhances its usability.

Overall, the proposed energy system can be very useful for future solar energy management and policy formulation in regions with distinct seasons, such as China, America, and Europe. It can solve the solar seasonal mismatch problem properly and has an exceeding performance in both the energy and economic perspectives. The main limitation of this energy system is the application in densely populated regions that lacks solar field area. Future research about this topic should be focused on system configuration optimization and the energy flexibility control strategy for the more efficient solar thermal utilization in the district energy systems.

Credit author statement

Datong Gao: Conceptualization, Methodology, Software, Validation, Formal analysis, Investigation, Data curation, Writing – original draft, Writing – review & editing, Visualization. **Trevor Hocksun Kwan**: Conceptualization, Writing – review & editing. **Maobin Hu**: Methodology, Writing – review & editing. **Gang Pei**: Conceptualization, Resources, Writing – review & editing, Supervision, Project administration, Funding acquisition.

Declaration of competing interest

The authors declare that they have no known competing financial interests or personal relationships that could have appeared to influence the work reported in this paper.

Acknowledgments

The study was sponsored by the National Key R&D Program of China (2018YFB1900602) and the National Natural Science Foundation of China (NSFC 51776193).

References

[1] Energy consumption statistics professional committee. China Building Energy Consumption Research Report (2020). China Association of Building Energy Efficiency; 2020.
[2] Qiu GD, Ma YY, Song WM, Cai WH. Comparative study on solar flat-plate collectors coupled with three types of reflectors not requiring solar tracking for space heating. Renew Energy 2021;169:104–16.
[3] Buonomano A, Forzano C, Kalogirou SA, Palombo A. Building-facade integrated solar thermal collectors: energy-economic performance and indoor comfort

simulation model of a water based prototype for heating, cooling, and DHW production. Renew Energy 2019;137:20–36.
[4] Berger M, Worlitschek J. A novel approach for estimating residential space heating demand. Energy 2018;159:294–301.
[5] Energy consumption statistics professional committee. China building energy consumption research report (2019). China Association of Building Energy Efficiency; 2019.
[6] Jia T, Dou PB, Chu P, Dai YJ. Proposal and performance analysis of a novel solar-assisted resorption-subcooled compression hybrid heat pump system for space heating in cold climate condition. Renew Energy 2020;150:1136–50.
[8] Chwieduk B, Chwieduk D. Analysis of operation and energy performance of a heat pump driven by a PV system for space heating of a single family house in polish conditions. Renew Energy 2021;165:117–26.
[9] Tian ZY, Perers B, Furbo S, Fan JH. Thermo-economic optimization of a hybrid solar district heating plant with flat plate collectors and parabolic trough collectors in series. Energy Convers Manag 2018;165:92–101.
[10] Hirvonen J, Rehman HU, Siren K. Techno-economic optimization and analysis of a high latitude solar district heating system with seasonal storage, considering different community sizes. Sol Energy 2018;162:472–88.
[11] Ministry of housing and urban-rural development of the People's Republic of China. 2020.
[12] Rismanchi B. District energy network (DEN), current global status and future development. Renew Sustain Energy Rev 2017;75:571–9.
[13] Lund H, Werner S, Wiltshire R, Svendsen S, Thorsen JE, Hvelplund F, et al. 4th Generation District Heating (4GDH) Integrating smart thermal grids into future sustainable energy systems. Energy 2014;68:1–11.
[14] Sayegh MA, Danielewicz J, Nannou T, Miniewicz M, Jadwiszczak P, Piekarska K, et al. Trends of European research and development in district heating technologies. Renew Sustain Energy Rev 2017;68:1183–92.
[15] Lund H, Moller B, Mathiesen BV, Dyrelund A. The role of district heating in future renewable energy systems. Energy 2010;35(3):1381–90.
[16] Carpaneto E, Lazzeroni P, Repetto M. Optimal integration of solar energy in a district heating network. Renew Energy 2015;75:714–21.
[17] Narula K, de Oliveira F, Villasmil W, Patel MK. Simulation method for assessing hourly energy flows in district heating system with seasonal thermal energy storage. Renew Energy 2020;151:1250–68.
[18] Rosato A, Ciervo A, Ciampi G, Scorpio M, Guarino F, Sibilio S. Impact of solar field design and back-up technology on dynamic performance of a solar hybrid heating network integrated with a seasonal borehole thermal energy storage serving a small-scale residential district including plug-in electric vehicles. Renew Energy 2020;154:684–703.
[19] Ochs F, Dahash A, Tosatto A, Janetti MB. Techno-economic planning and construction of cost-effective large-scale hot water thermal energy storage for Renewable District heating systems. Renew Energy 2020;150:1165–77.
[20] Chang C, Nie BJ, Leng GH, Li C, She XH, Peng XD, et al. Influences of the key characteristic parameters on the thermal performance of a water pit seasonal thermal storage. Energy Procedia 2017;142:495–500.
[21] Paiho S, Hoang H, Hukkalainen M. Energy and emission analyses of solar assisted local energy solutions with seasonal heat storage in a Finnish case district. Renew Energy 2017;107:147–55.
[22] Jradi M, Veje C, Jorgensen BN. Performance analysis of a soil-based thermal energy storage system using solar-driven air-source heat pump for Danish buildings sector. Appl Therm Eng 2017;114:360–73.
[23] Panno D, Buscemi A, Beccali M, Chiaruzzi C, Cipriani G, Ciulla G, et al. A solar assisted seasonal borehole thermal energy system for a non-residential building in the Mediterranean area. Sol Energy 2019;192:120–32.
[24] Permyakova A, Wang SJ, Courbon E, Nouar F, Heymans N, D'Ans P, et al. Design of salt-metal organic framework composites for seasonal heat storage applications. J Mater Chem 2017;5(25):12889–98.
[25] Guelpa E, Marincioni L, Deputato S, Capone M, Amelio S, Pochettino E, et al. Demand side management in district heating networks: a real application. Energy 2019;182:433–42.
[26] Chen YB, Xu P, Chen Z, Wang HX, Sha HJ, Ji Y, et al. Experimental investigation of demand response potential of buildings: combined passive thermal mass and active storage. Appl Energy 2020:280.
[27] Guelpa E, Verda V. Demand response and other demand side management techniques for district heating: a review. Energy 2021:219.
[28] Christensen MH, Li RL, Pinson P. Demand side management of heat in smart homes: living-lab experiments. Energy 2020:195.
[29] Amasyali K, El-Gohary NM. Real data-driven occupant-behavior optimization for reduced energy consumption and improved comfort. Appl Energy 2021:302.
[30] Reynolds J, Rezgui Y, Kwan A, Piriou S. A zone-level, building energy optimisation combining an artificial neural network, a genetic algorithm, and model predictive control. Energy 2018;151:729–39.
[31] Luo X, Liu YF, Feng PA, Gao Y, Guo ZX. Optimization of a solar-based integrated energy system considering interaction between generation, network, and demand side. Appl Energy 2021:294.
[32] Reynolds J, Ahmad MW, Rezgui Y, Hippolyte JL. Operational supply and demand optimisation of a multi-vector district energy system using artificial neural networks and a genetic algorithm. Appl Energy 2019;235:699–713.
[33] Le Dreau J, Heiselberg P. Energy flexibility of residential buildings using short term heat storage in the thermal mass. Energy 2016;111:991–1002.
[34] Vivian J, Quaggiotto D, Zarrella A. Increasing the energy flexibility of existing district heating networks through flow rate variations. Appl Energy 2020:275.
[35] Vandermeulen A, van der Heijde B, Helsen L. Controlling district heating and cooling networks to unlock flexibility: a review. Energy 2018;151:103–15.
[36] Liu C, Han W, Wang Z, Zhang N, Kang Q, Liu M. Proposal and assessment of a new solar space heating system by integrating an absorption-compression heat pump. Appl Energy 2021;294:116966.
[37] Arabkoohsar A, Andresen GB. Supporting district heating and cooling networks with a bifunctional solar assisted absorption chiller. Energy Convers Manag 2017;148:184–96.
[38] Arabkoohsar A, Andresen GB. A smart combination of a solar assisted absorption chiller and a power productive gas expansion unit for cogeneration of power and cooling. Renew Energy 2018;115:489–500.
[39] Arabkoohsar A, Sadi M. A solar PTC powered absorption chiller design for Co-supply of district heating and cooling systems in Denmark. Energy 2020;193:945–57.
[40] Guo F, Zhu XY, Zhang JY, Yang XD. Large-scale living laboratory of seasonal borehole thermal energy storage system for urban district heating. Appl Energy 2020:264.
[41] Tian ZY, Perers B, Furbo S, Fan JH. Annual measured and simulated thermal performance analysis of a hybrid solar district heating plant with flat plate collectors and parabolic trough collectors in series. Appl Energy 2017;205:417–27.
[42] National Development and Reform Commission of China. Typical electricity load curve of each provincial grid. National Energy Administration; 2020.
[43] Cioccolanti L, Hamedani SR, Villarini M. Environmental and energy assessment of a small-scale solar Organic Rankine Cycle trigeneration system based on Compound Parabolic Collectors. Energy Convers Manag 2019;198.
[44] Freeman J, Hellgardt K, Markides CN. An assessment of solar-powered organic Rankine cycle systems for combined heating and power in UK domestic applications. Appl Energy 2015;138:605–20.
[45] Freeman J, Hellgardt K, Markides CN. Working fluid selection and electrical performance optimisation of a domestic solar-ORC combined heat and power system for year-round operation in the UK. Appl Energy 2017;186:291–303.
[46] Liu M, Tay NHS, Bell S, Belusko M, Jacob R, Will G, et al. Review on concentrating solar power plants and new developments in high temperature thermal energy storage technologies. Renew Sustain Energy Rev 2016;53:1411–32.
[47] Gao DT, Gao GT, Cao JY, Zhong S, Ren X, Dabwan YN, et al. Experimental and numerical analysis of an efficiently optimized evacuated flat plate solar collector under medium temperature. Appl Energy 2020;269.
[48] Ministry of Housing and Urban-Rural Development of the People Republic of China. Design code for heating ventilation and air conditioning of civil buildings. Chinese National Standard; 2012.
[49] Su W, Zhao L, Deng S, Xu WC, Yu ZX. A limiting efficiency of subcritical Organic Rankine cycle under the constraint of working fluids. Energy 2018;143:458–66.
[50] Li J, Gao G, Kutlu C, Liu K, Pei G, Su Y, et al. A novel approach to thermal storage of direct steam generation solar power systems through two-step heat discharge. Appl Energy 2019;236:81–100.
[51] Ehyaei MA, Ahmadi A, Assad ME, Rosen MA. Investigation of an integrated system combining an Organic Rankine Cycle and absorption chiller driven by geothermal energy: energy, exergy, and economic analyses and optimization. J Clean Prod 2020:258.
[52] Landelle A, Tauveron N, Haberschill P, Revellin R, Colasson S. Organic Rankine cycle design and performance comparison based on experimental database. Appl Energy 2017;204:1172–87.
[53] Pang KC, Chen SC, Hung TC, Feng YQ, Yang SC, Wong KW, et al. Experimental study on organic Rankine cycle utilizing R245fa, R123 and their mixtures to investigate the maximum power generation from low-grade heat. Energy 2017;133:636–51.
[54] Sharafeldin MA, Grof G, Mahian O. Experimental study on the performance of a flat-plate collector using WO3/Water nanofluids. Energy 2017;141:2436–44.
[55] Said Z, Saidur R, Rahim NA. Energy and exergy analysis of a flat plate solar collector using different sizes of aluminium oxide based nanofluid. J Clean Prod 2016;133:518–30.
[56] Chi FA, Xu LM, Pan JJ, Wang RN, Tao YK, Guo YA, et al. Prediction of the total day-round thermal load for residential buildings at various scales based on weather forecast data. Appl Energy 2020:280.
[57] EnergyPlus weather data. 2020.
[58] Technical standard for solar heating system. The Ministry of housing and urban-rural development of the People's Republic of China. 2019.
[59] Kalogirou SA. Solar energy engineering: processes and systems. second ed. United States of America: Elsevier Inc.; 2014.
[60] Bird TJ, Jain N. Dynamic modeling and validation of a micro-combined heat and power system with integrated thermal energy storage. Appl Energy 2020:271.
[61] Aziz F, Salim MS, Kim MH. Performance analysis of high temperature cascade organic Rankine cycle coupled with water heating system. Energy 2019;170:954–66.
[62] Kim DK, Lee JS, Kim J, Kim MS, Kim MS. Parametric study and performance evaluation of an organic Rankine cycle (ORC) system using low-grade heat at temperatures below 80 degrees C. Appl Energy 2017;189:55–65.
[63] Li S, Ma HJ, Li WY. Dynamic performance analysis of solar organic Rankine cycle with thermal energy storage. Appl Therm Eng 2018;129:155–64.

[64] Abo-Elfadl S, Hassan H, El-Dosoky MF. Energy and exergy assessment of integrating reflectors on thermal energy storage of evacuated tube solar collector-heat pipe system. Sol Energy 2020;209:470–84.
[65] Balaji K, Iniyan S, Swami MV. Exergy, economic and environmental analysis of forced circulation flat plate solar collector using heat transfer enhancer in riser tube. J Clean Prod 2018;171:1118–27.
[66] Rezaie B, Reddy BV, Rosen MA. Exergy analysis of thermal energy storage in a district energy application. Renew Energy 2015;74:848–54.
[67] Lake A, Rezaie B, Beyerlein S. Review of district heating and cooling systems for a sustainable future. Renew Sustain Energy Rev 2017;67:417–25.
[68] Kelly KA, McManus MC, Hammond GP. An energy and carbon life cycle assessment of industrial CHP (combined heat and power) in the context of a low carbon UK. Energy 2014;77:812–21.
[69] Tulus V, Boer D, Cabeza LF, Jimenez L, Guillen-Gosalbez G. Enhanced thermal energy supply via central solar heating plants with seasonal storage: a multi-objective optimization approach. Appl Energy 2016;181:549–61.
[70] Calise F, d'Accadia MD, Palombo A. Transient analysis and energy optimization of solar heating and cooling systems in various configurations. Sol Energy 2010;84(3):432–49.
[71] Richard Turton JAS, Bhattacharyya Debangsu, Wallace B, Whiting. Analysis, synthesis and design of chemical processes. In: International series in the physical and chemical engineering sciences. fifth ed. 2018.
[72] Alshammari F, Karvountzis-Kontakiotis A, Pesyridis A, Usman M. Expander technologies for automotive engine organic rankine cycle applications. Energies 2018;11(7).
[73] Lecompte S, Huisseune H, van den Broek M, De Schampheleire S, De Paepe M. Part load based thermo-economic optimization of the Organic Rankine Cycle (ORC) applied to a combined heat and power (CHP) system. Appl Energy 2013;111:871–81.
[74] Quoilin S, Declaye S, Tchanche BF, Lemort V. Thermo-economic optimization of waste heat recovery Organic Rankine Cycles. Appl Therm Eng 2011;31(14–15):2885–93.
[75] Li LX, Mu HL, Li N, Li M. Economic and environmental optimization for distributed energy resource systems coupled with district energy networks. Energy 2016;109:947–60.
[76] Chen T, Zhuge WL, Zhang YJ, Zhang L. A novel cascade organic Rankine cycle (ORC) system for waste heat recovery of truck diesel engines. Energy Convers Manag 2017;138:210–23.
[77] Moravej M, Bozorg MV, Guan Y, Li LKB, Doranehgard MH, Hong K, et al. Enhancing the efficiency of a symmetric flat-plate solar collector via the use of rutile TiO2-water nanofluids. Sustainable Energy Technologies and Assessments; 2020. p. 40.
[78] Gungor A, Erbay Z, Hepbasli A. Exergetic analysis and evaluation of a new application of gas engine heat pumps (GEHPs) for food drying processes. Appl Energy 2011;88(3):882–91.
[79] Zhang Y, Zhao DW, Yu F, Yang C, Lou JW, Liu YM, et al. Floating rGO-based black membranes for solar driven sterilization. Nanoscale 2017;9(48):19384–9.
[80] Ozturk HH. Comparison of energy and exergy efficiencies of an underground solar thermal storage system. Int J Energy Res 2004;28(4):341–53.
[81] Sibbitt B, McClenahan D, Djebbar R, Thornton J, Wong B, Carriere J, et al. The performance of a high solar fraction seasonal storage district heating system - five years of operation. Energy Procedia 2012;30:856–65.
[82] Hirvonen J, Siren K. A novel fully electrified solar heating system with a high renewable fraction - optimal designs for a high latitude community. Renew Energy 2018;127:298–309.
[83] Xu J, Wang RZ, Li Y. A review of available technologies for seasonal thermal energy storage. Sol Energy 2014;103:610–38.
[84] Rehman HU, Hirvonen J, Siren K. Performance comparison between optimized design of a centralized and semi-decentralized community size solar district heating system. Appl Energy 2018;229:1072–94.